

A Heterobimetallic Approach To Stabilize the Elusive Disulfur Radical Trianion (“Subsulfide”) S₂³⁻

Shenglai Yao,^[a] Peter Hrobárik,^[b, c] Florian Meier,^[b] Robert Rudolph,^[a] Eckhard Bill,^[d] Elisabeth Irran,^[a] Martin Kaupp,^{*,[b]} and Matthias Driess^{*,[a]}

Dedicated to Professor Karl Wieghardt on the occasion of his 70th birthday

Abstract: A unique heterobimetallic disulfur monoradical, complex **2**, with a diamond-shaped {NiS₂Pt} core has been synthesized by two-electron reduction of a supersulfido-(nacnac)-nickel(II) complex (nacnac = β-diketiminato) with [Pt(Ph₃P)₂(η²-C₂H₄)] as a platinum(0) source and isolated in 82% yield. Strikingly, the results of DFT calculations in accordance with spectroscopic (EPR, paramagnetic NMR) and structural features of the complex revealed that the bonding sit-

uation of the S₂ ligand is between the elusive “half-bonded” S₂ radical trianion (S₂³⁻) and two separated S²⁻ ligands. Accordingly, the Ni^{II} center is partially oxidized, whereas the Pt^{II} site is redox innocent. The complex can be reversibly oxidized to the corresponding Ni,Pt-disulfido monocation, com-

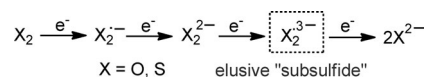
pound **3**, with a S–S single bond, and reacts readily with O₂ to form the corresponding superoxonickel(II) and disulfidoplatinum(II) (**4**) complexes. These compounds have been isolated in crystalline form and fully characterized, including IR and multi-nuclear NMR spectroscopy as well as ESI mass spectrometry. The molecular structures of compounds **2–4** have been confirmed by single-crystal X-ray crystallography.

Keywords: dichalcogens • nickel • oxidation states • platinum • redox ligands

Introduction

Akin to the metal-mediated activation of dioxygen, the reduction of elemental sulfur (commonly S_n rings such as S₈) with metals can lead to different metal disulfide species bearing the supersulfide (S₂⁻), disulfide (S₂²⁻), or bridging sulfide ligand (S²⁻). Reductive cleavage of a dichalcogen

moiety X₂ (X = O, S) into two chalcogenide centers (X²⁻) requires in total four electrons (Scheme 1).



Scheme 1. Step-by-step reduction of a dichalcogen X₂.

[a] Dr. S. Yao, Dipl.-Chem. R. Rudolph, Dr. E. Irran, Prof. Dr. M. Driess
Technische Universität Berlin
Department of Chemistry
Metalorganics and Inorganic Materials
Sekt. C2, Strasse des 17. Juni 135
10623 Berlin (Germany)
E-mail: matthias.driess@tu-berlin.de

[b] Dr. P. Hrobárik, Dipl.-Chem. F. Meier, Prof. Dr. M. Kaupp
Technische Universität Berlin
Department of Chemistry: Theoretical Chemistry
Sekt. C7, Strasse des 17. Juni 135
10623 Berlin (Germany)
E-mail: martin.kaupp@tu-berlin.de

[c] Dr. P. Hrobárik
Institute of Inorganic Chemistry
Slovak Academy of Sciences
Dúbravská cesta 9
84536 Bratislava (Slovakia)

[d] Dr. E. Bill
Max-Planck Institute of Chemical Energy Conversion
Stiftsstrasse 34-36
45470 Müllheim/Ruhr (Germany)

Supporting information for this article is available on the WWW under <http://dx.doi.org/10.1002/chem.201203642>.

Understanding these step-by-step transformations in the environment of transition metals is of considerable interest because of their importance in catalytic redox processes and biorelevance.^[1] Although the chemistry of transition-metal complexes containing dichalcogenide X₂²⁻ and bridging X²⁻ ligands has been well established, only a few striking examples featuring a superchalcogenide X₂⁻ ligand could be isolated and structurally characterized.^[2,3] Realization of a dichalcogenide radical ligand X₂³⁻ (“subchalcogenides”) with a X–X σ bond order of 0.5 (similar to H₂⁻) represents an even more ambitious task because dichalcogen X₂ⁿ⁻ ligands are expected to act as non-innocent redox ligands.

Recently, a striking copper complex with a {Cu₃S₂}³⁺ core engendered a vivid debate about the interpretation of its electronic structure (Figure 1).^[4] Unlike the oxygen congener {Cu₃O₂}³⁺,^[5] which has a local C_{2v} symmetry originating from shorter Cu–O distances for one Cu atom than for the other two, and which features unambiguously two O²⁻ ions, the {Cu₃S₂}³⁺ core adopts a local D_{3h} symmetry and contains a S₂ moiety with a S⋯S distance of 2.69 Å. It may be consid-

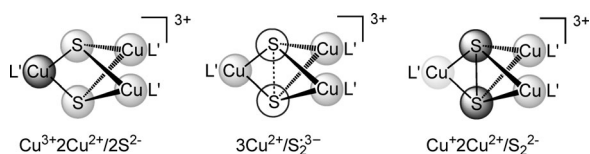
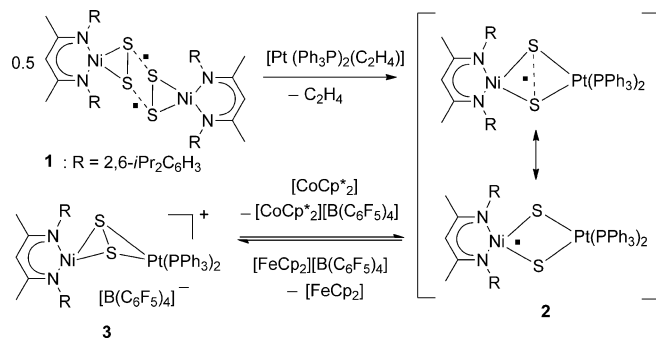


Figure 1. Possible S–S bonding interactions in a $\{Cu_3S_2\}^{3+}$ core. $L' = N,N,N',N'$ -tetramethylethylenediamine (tmeda).

ered as a species having a weak attractive $S \cdots S$ interaction in formal accordance with S_2^{3-} (“subulfide”) character^[4] (see, very recent discussion of a possible Se_2^{3-} -type ligand in a $\{Ni_2Se_2\}$ complex^[6]). However, X-ray adsorption spectroscopy and computational studies by using various electronic-structure analysis approaches clearly demonstrated the intrinsic difficulty in assigning the formal oxidation states to Cu and S in the system, owing to the high symmetry of the $\{Cu_3S_2\}^{3+}$ core, the large covalent character of the Cu–S bonds, and significant $S,S \rightarrow Cu(3d)$ donation.^[4] The latter controversy over the oxidation state encouraged us to develop a less symmetric M,M' -heterobimetallic disulfur complex, featuring a diamond-shaped $\{M(S_2)M'\}$ core (see Scheme 2) and an electron count, which might facilitate the formation of the elusive disulfur radical ligand S_2^{3-} .



Scheme 2. Formation of the $\{Ni(S_2)Pt\}$ radical complex **2** from reaction of supersulfidonickel(II) **1** with $[Pt(Ph_3P)_2(\eta^2-C_2H_4)]$ and its reversible redox conversion into **3**. The electronic structure of **2** is described by two resonance forms with spin densities residing at the sulfur and the nickel atoms, respectively.

As a promising approach we pursued the synthesis of a heterobimetallic S_2^{3-} complex through a two-electron reduction of the supersulfido ligand in the dimeric supersulfido-(nacnac)nickel(II) complex **1** (nacnac = β -diketiminato); this starting material is readily accessible by reaction of the corresponding nickel(I) precursor $[\{Ni(nacnac)\}_2] \cdot toluene$ ^[7] with elemental sulfur.^[3c] After a series of unsuccessful experiments employing several potential reducing agents (e.g., Mg, Ni^0 , and Pd^0 complexes), we learned that platinum(0) in $[Pt(Ph_3P)_2(\eta^2-C_2H_4)]$ can serve as a reliable two-electron reducing agent to achieve the desired reduction of the supersulfido complex **1** to give compound **2** (Scheme 2). Here, we report the synthesis, characterization, and reactivity of the unique $\{Ni(S_2)Pt\}$ radical complex **2**. Our theoretical investi-

gations revealed that complex **2** shows significant S_2^{3-} radical character ($\approx 41\%$), very similar to the $\{Cu_3S_2\}^{3+}$ system but with surprisingly unsymmetrical atomic spin densities at the two sulfur atoms (34 vs. 7%). In addition, our calculations show that “pure” S_2^{3-} radical character would be present upon replacement of the redox non-innocent Ni^{II} in complex **2** by redox innocent Zn^{II} .

Results and Discussion

Synthesis of radical complex 2: Treatment of **1** with two equivalents of bis(triphenylphosphine)ethylene platinum(0) in toluene at $-20^\circ C$ resulted in the formation of complex **2**, indicated by the color change from dark brown to dark green (Scheme 2). After workup, complex **2** could be isolated in 82% yield as dark green crystals. Its composition was proven by elemental analysis and ESI mass spectrometry. Its molecular structure has been established by single-crystal X-ray diffraction analysis (Figure 2).

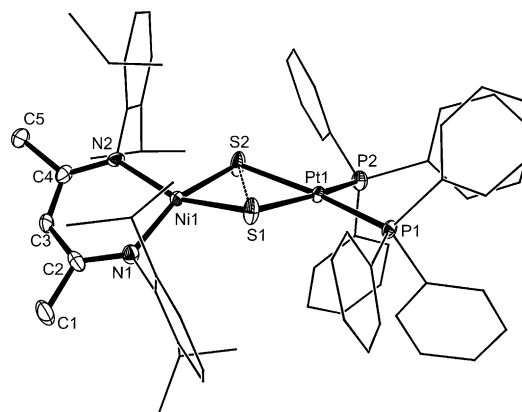


Figure 2. Molecular structure of complex **2**. Thermal ellipsoids are drawn at 50% probability level. Hydrogen atoms are omitted. Two independent molecules are in the unit cell. Selected distances [\AA] and angles [$^\circ$]: molecule 1: $S1 \cdots S2$ 2.71(2), $Pt1-P1$ 2.283(2), $Pt1-P2$ 2.301(2), $Pt1-S1$ 2.305(2), $Pt1-S2$ 2.314(2), $Ni1-N1$ 1.942(6), $Ni1-N2$ 1.946(5), $Ni1-S1$ 2.153(2), $Ni1-S2$ 2.164(2), $P1-P1-P2$ 100.49(6), $P1-Pt1-S1$ 94.42(6), $P2-Pt1-S1$ 163.53(6), $P1-Pt1-S2$ 166.17(6), $P2-Pt1-S2$ 93.34(6), $S1-Pt1-S2$ 71.83(6), $N1-Ni1-N2$ 93.9(2), $S1-Ni1-S2$ 77.75(7), $Ni1-S1-Pt1$ 103.90(7), $Ni1-S2-Pt1$ 103.26(7); molecule 2: $S1 \cdots S2$ 2.70(2), $Pt1-P2$ 2.286(2), $Pt1-P1$ 2.299(2), $Pt1-S1$ 2.302(2), $Pt1-S2$ 2.307(2), $Ni1-N2$ 1.931(5), $Ni1-N1$ 1.948(6), $Ni1-S2$ 2.150(2), $Ni1-S1$ 2.162(2), $P2-Pt1-P1$ 100.12(6), $P2-Pt1-S1$ 166.37(6), $P1-Pt1-S1$ 93.49(6), $P2-Pt1-S2$ 94.86(6), $P1-Pt1-S2$ 163.76(6), $S1-Pt1-S2$ 71.71(6), $N2-Ni1-N1$ 93.5(2), $S2-Ni1-S1$ 77.51(7), $Ni1-S1-Pt1$ 102.29(7), $Ni1-S2-Pt1$ 102.48(7).

The Ni–S distances in **2** (2.150(2)–2.164(2) \AA) are close to those found in **1** (2.163(1), 2.166(1) \AA) and slightly shorter than those observed for the butterfly-like complex with a $\{Ni^{II}_2(\mu-\eta^2:\eta^2-S_2)\}$ core, ranging from 2.193(1) to 2.205(1) \AA .^[3c] The Pt–S distances in **2** (2.302(2) and 2.314(2) \AA), are similar to the corresponding values observed in complexes with a $\{Pt_2(\mu-S)_2\}$ core (2.33–2.35 \AA),^[8a–c] and the d^8 -Pt center is square-planar coordinat-

ed. The most interesting geometric features are the non-planar tetra-coordination of the Ni site and the S...S distance of approximately 2.71 Å. The latter is much shorter than the distances observed in complexes with a {Pt₂(μ-S)₂} core (3.060–3.134 Å).^[8a–d] It is also shorter than that observed for the naphthalene-based bis(phosphine)nickel(II) complex with a {Ni₂(μ-S)₂} core (2.839(4) Å),^[8e] but significantly longer than the values observed for complexes with a {Ni₂(η²:η²-S₂)} core (2.051(1)–2.054(2) Å).^[3c]

Complex **2** is paramagnetic in the solid state as well as in solution. Magnetic measurement performed in C₆D₆ (by using the Evans method^[9]) revealed a μ_{eff} value of 1.83 μ_B at room temperature, which is close to the spin-only value of one unpaired electron. Correspondingly, the X-band EPR spectrum recorded at 10 K from a frozen solution of complex **2** in THF (Figure 3) shows three rhombically split de-

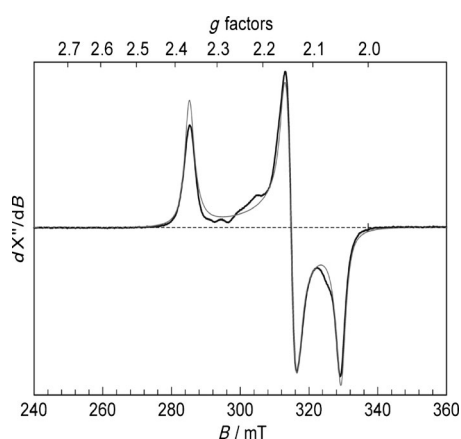


Figure 3. X-band EPR spectrum of complex **2** in a frozen THF solution measured at 10 K (frequency 9.4390 GHz, power 0.2 mW, modulation 1 mT per 100 kHz). The gray line is the result of a powder simulation with anisotropic *g* values (*g*=2.365, 2.143, 2.048) and line widths ($\Gamma=38 \times 10^{-4}$, 31×10^{-4} , 38×10^{-4} cm⁻¹).

rivative lines (*g*=2.365, 2.143, 2.048) with an average *g* value of 2.189 (corresponding to μ_{eff}=1.896 μ_B). Both, the ¹H and the ³¹P NMR spectrum of **2** measured in C₆D₆ exhibit paramagnetically shifted resonances (see the Supporting Information), the latter with a broad signal at δ = -415 ppm. Among the ¹H NMR shifts, the most pronounced shielding due to the paramagnetic nature of the complex is experienced at the γ position of the nacnac ligand (δ = -39.3 ppm), indicating some spin delocalization from the {Ni₂Pt} core to this fragment.

DFT calculations for complex 2: Structure optimizations on complex **2** at the RI-BP86/def2-TZVP level (see Computational methods section) provide good agreement with the X-ray diffraction data (*d*(S–S)=2.717, *d*(Ni–S)=2.136, 2.201, *d*(Pt–S)=2.338, 2.342 Å; see Table S2 in the Supporting Information). Subsequent state-of-the-art DFT calculations of paramagnetic NMR chemical shifts^[10] at this structure reproduce well the experimentally observed ¹H and

³¹P NMR signals and aid in the spectra assignment (Tables S8 and S9 as well as Figure S1 in the Supporting Information). It turned out that the best agreement with experimental NMR shifts was obtained with a modified B3LYP** functional with reduced exact-exchange admixture (10%),^[11] thus avoiding excessive spin contamination (see Tables S5 and S8 as well as Figure S3 in the Supporting Information). This functional was used subsequently to establish spin-density distributions and the electronic structure of complex **2** and of related complexes. The electronic *g* tensor of **2** is also well reproduced at this level, with *g*_{iso}=2.162 and *g*-tensor principal values of 2.085, 2.166, and 2.235. Closer analysis (Table S7 in the Supporting Information) reveals that it is dominated by Ni spin-orbit coupling, thus confirming non-negligible spin density at this metal center.

Various approaches have been used to analyze the electronic structure of complex **2**, in an attempt to assign “physical oxidation states” to Ni, Pt, and the bridging S₂ unit. To have a “pure” S₂³⁻ subsulfide reference point, the simple model complex Na₃S₂ has been optimized and analyzed at the same levels, whereas the cation [**2**]⁺ is our disulfide S₂²⁻ reference point. Additional calculations on the analogues **2**-Pt and **2**-Zn (replacing Ni in complex **2** by Pt and by tetrahedrally coordinated Zn, respectively), the cation [**2**-Zn]⁺, the anion [**2**-Zn]⁻, on [Na₃S₂]^{+/-}, and on the [(tmeda)₃-Cu₃S₂]³⁺ complex^[4] (see Figure 1) provide further points for comparison.

Spin-density distributions (Figure 4, Table 1) provide a particularly informative view: the natural orbital population (NPA) spin densities near 0.5 on both sulfur atoms, and rather small spin densities on the metal fragments in Na₃S₂ and **2**-Zn agree with expectations for an S₂³⁻ radical disulfide

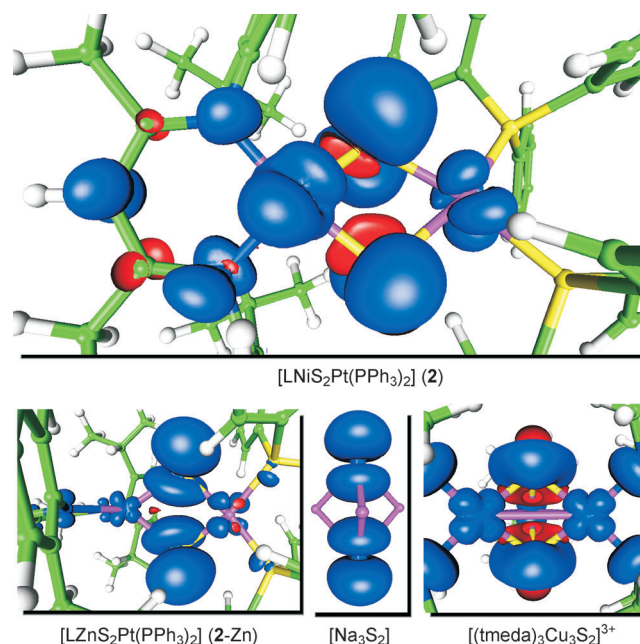


Figure 4. Spin-density isosurface plots (±0.001 a.u.) in the vicinity of the S₂ unit in pertinent metal complexes (B3LYP**/TZVP results). Positive spin density is indicated in blue, negative spin density in red.

Table 1. Crucial NPA atomic spin densities in selected systems.^[a]

Complex		NPA spin densities of {MS(1)S(2)M'} core atoms			
		S(1)	S(2)	M	M' = Pt
[LNiS ₂ Pt(PPh ₃) ₂]	2	0.346	0.070	0.499	0.028
		0.352 ^[b]	0.123 ^[b]	0.454 ^[b]	0.026 ^[b]
[LZnS ₂ Pt(PPh ₃) ₂]	2-Zn	0.506	0.429	0.000	0.011
[LPtS ₂ Pt(PPh ₃) ₂]	2-Pt	0.446	0.282	0.204	0.058
[(tmeda) ₃ Cu ₃ S ₂] ³⁺		0.240	0.240	0.272 ^[c]	–
[Na ₃ S ₂]		0.521	0.521	–0.014 ^[c]	–

[a] B3LYP**/TZVP//BP86/def2-TZVP results (see the Computational methods section). M atoms marked in bold. L stands for the CH₂[(CMe)(2,6-*i*-Pr₂C₆H₃N)]₂ ligand, denoted also as “nacnac” throughout the text. [b] Atomic spin densities calculated for the crystal structure of **2** with optimized hydrogen positions. [c] Average values over all metal atoms (M = Cu or Na).

ion. These two compounds provide clear-cut models for such an oxidation state. The S–S distance in complex **2** (Table 2) is actually shorter than those in the two reference models and very similar to the values obtained for [(tmeda)₃Cu₃S₂]³⁺. This suggests that the Coulombic S–S repulsion is better compensated due to an increased covalency of the M–S bond, as also confirmed by NPA charges (Table 2). Strikingly, the sulfur atoms in **2** exhibit much lower and asymmetrical sulfur spin densities, overall also somewhat less on average than that of the copper system (Table 1). The inequality clearly reflects the asymmetric bonding of the disulfur ligand to the non-planar tetra-coordinate Ni center. Even based on the crystal structure with its more similar Ni–S distances (see Ni–S distances in Table S2 in Supporting Information), the spin density remains strongly asymmetric (see Table 1). This is due to a twisting of the S₂ ligand relative to the N–Ni–N plane of the (nacnac)Ni complex fragment: The S1 atom is significantly outside the plane, leading to a larger Ni–S1 than Ni–S2 covalency, consistent with respective NPA charges (see

Table 2. Optimized S...S distances in [Å], S...S Mayer bond orders (MBO), and NPA atomic charges in pertinent complexes.^[a]

Complex		<i>d</i> (S...S)	MBO	NPA charges			
				S(1)	S(2)	M	Pt
radical disulfides, S ₂ ³⁻							
[LNiS ₂ Pt(PPh ₃) ₂]	2	2.717	0.215	–0.425	–0.555	0.875	0.129
[LZnS ₂ Pt(PPh ₃) ₂]	2-Zn	2.895	0.339	–0.702	–0.762	1.546	0.141
[LPtS ₂ Pt(PPh ₃) ₂]	2-Pt	2.943	0.218	–0.350	–0.459	0.542	0.155
[(tmeda) ₃ Cu ₃ S ₂] ³⁺		2.703	0.206	–1.267	–1.267	1.020 ^[b]	–
[Na ₃ S ₂]		3.421	0.430	–0.675	–0.675	0.845 ^[b]	–
disulfides, S ₂ ²⁻							
[LNiS ₂ Pt(PPh ₃) ₂] ⁺	[2] ⁺	2.065	0.947	–0.168	–0.180	0.777	0.103
[LZnS ₂ Pt(PPh ₃) ₂] ⁺	[2-Zn] ⁺	2.141	0.942	–0.389	–0.407	1.564	0.112
[Na ₃ S ₂] ⁺		2.226	0.894	–0.931	–0.931	0.954 ^[b]	–
sulfides, 2S ²⁻							
[LZnS ₂ Pt(PPh ₃) ₂] ⁻	[2-Zn] ⁻	3.278	0.052	–1.025	–1.037	1.511	0.159
[Na ₃ S ₂] ⁻		4.102	0.042	–1.533	–1.533	0.689 ^[b]	–

[a] B3LYP**/TZVP//BP86/def2-TZVP results (see the Computational methods section). M atoms marked in bold. L stands for the CH₂[(CMe)(2,6-*i*-Pr₂C₆H₃N)]₂ ligand. [b] Average values over all metal atoms (M = Cu or Na).

Table 2). The twisting survives even in smaller model complexes, in which the alkyl and aryl substituents on the nacnac ligand and on the Pt-bound phosphine ligands were replaced by hydrogen atoms (see the Supporting Information). This indicates that the asymmetry is not caused by steric congestion but electronically preferred. Indeed, the twisting is related to a partial oxidation of the Ni^{II} center beyond the d⁸ configuration and respective partial reduction of the disulfur ligand to a state between the S₂³⁻ and two S²⁻ moieties (Scheme 2). A genuine tetra-coordinate, low-spin Ni^{II} has no reason to become non-planar. Consequently, the twisting is absent in small truncated models of the one-electron-oxidized cationic complex [**2**]⁺ (see compound **3** below), which represents a true d⁸ Ni^{II} situation. Consistent with this picture, the Ni charge in complex **2** is clearly more positive than that in [**2**]⁺. We furthermore note, that only the spin densities of Na₃S₂ and of the Cu complex are consistent with a hole in the σ* orbital of the S–S bond. In all other cases, the lower symmetry leads to substantial contributions of p_π-type atom orbitals (AOs) to the SOMO and thus to the spin density on the S₂ unit (see Figure 4 and Tables S14 and S15 in the Supporting Information).

Compared to the copper system, all other systems exhibit much less spin polarization at a given computational level (Figure 4), clearly ruling out a broken-symmetry-type wave function discussed by Berry^[4d] for [(tmeda)₃Cu₃S₂]³⁺ (see also natural orbital populations in Table S13 in the Supporting Information).

We have used further measures in an attempt to establish the presence or absence of attractive S...S interactions in complex **2** and in the other compounds studied. Neither in the electron localization function (ELF), the electron localizability indicator (ELI), or in the Laplacian of the electron density, complex **2** exhibits an S–S bonding attractor (see Table S16 in the Supporting Information). However, such an attractor is also absent in **2-Zn** or in Na₃S₂, which may be considered as “pure” S₂³⁻ examples, whereas such attractors are clearly present in any disulfide complex we looked at (see the Supporting Information). It is thus difficult to establish the presence of S–S bonding in the radical disulfide trianion species by such real-space quantities. On the other hand, Mayer bond orders (Table 2) indicate non-negligible but weak S–S bonding in complex **2** as well as in [(tmeda)₃Cu₃S₂]³⁺, thus confirming a situation between a genuine S₂³⁻ radical trianion situation and two separated S²⁻ bridging ligands, but with unsymmetrical sulfur spin-density distribution and bonding situation for complex **2**. However, it

is clearly not a broken-symmetry case, and the spin polarization is much weaker. We note in passing that weak S...S interactions have also been discussed in detail in S_4^{2-} -type ligands in certain rhodium and iridium complexes and related model systems.^[4b,12]

Reactivity of radical complex 2: The one-electron oxidation of complex **2** with $[\text{FeCp}_2][\text{B}(\text{C}_6\text{F}_5)_4]$ (Cp=cyclopentadienyl) leads to the formation of the ion-separated pair **3**, which has been readily obtained as black crystals in 89% yield (Scheme 2). Compound **3** is diamagnetic and displays reasonable resonances in the ^1H NMR spectrum. The ^{31}P nucleus of the PPh_3 ligand resonates at $\delta=11.6$ ppm with ^{195}Pt satellites ($^1J(\text{P,Pt})=3963$ Hz). The composition of **3** has been further confirmed by ^{13}C and ^{19}F NMR as well as by elemental analysis. Compound **3** is marginally soluble in hydrocarbons but well soluble in THF and dichloromethane. The molecular structure of **3** has also been established by X-ray diffraction analysis (Figure 5). No significant interac-

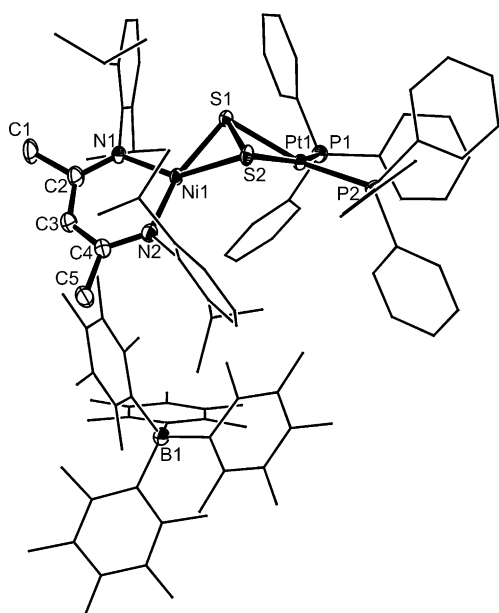
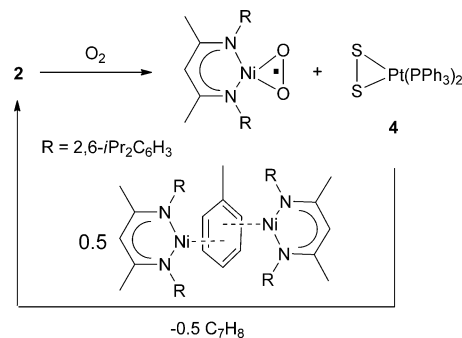


Figure 5. Molecular structure of **3**. Thermal ellipsoids are drawn at 50% probability level. Hydrogen atoms are omitted. Selected distances [Å] and angles [°]: S1–S2 2.058(3), Pt1–P2 2.254(2), Pt1–P1 2.286(3), Pt1–S2 2.344(2), Pt1–S1 2.360(2), Ni1–N1 1.880(7), Ni1–N2 1.881(7), Ni1–S1 2.196(2), Ni1–S2 2.231(2), P2–Pt1–P1 100.43(9), P2–Pt1–S2 104.81(8), P1–Pt1–S2 154.58(8), P2–Pt1–S1 151.27(9), P1–Pt1–S1 103.12(8), S2–Pt1–S1 51.90(8), N1–Ni1–N2 97.7(3), S1–Ni1–S2 55.40(9), Ni1–S1–Pt1 100.10(8), Ni1–S2–Pt1 99.55(9).

tions were observed between the counterions (shortest Ni–F distance: 5.184 Å and shortest Pt–F distance: 6.347 Å). The cation adopts a conformation quite similar to that of its precursor **2** except for the folding angle of the four-membered Ni_2Pt ring (62.0° in **3** vs. 17.0 and 23.2° in **2**). However, the S–S distance in **3** (2.0583(3) Å), which is significantly shorter than the corresponding value found in **2** (2.70 or 2.71 Å), falls in the ordinary range of S–S single bond lengths. Thus,

through one-electron oxidation, the Ni,Pt-subsulfido complex **2** was converted into the Ni,Pt-disulfido cation in **3** as confirmed by electronic-structure analyses (see data for $[\mathbf{2}]^+$ in Table 2). Interestingly, the oxidation is reversible as proven by the chemical reduction of **3** with one equivalent of bis(η^5 -pentamethylcyclopentadienyl)cobalt, affording complex **2** in 73% yield (see Scheme 2).



Scheme 3. Reaction of complex **2** with dioxygen to form the superoxo-nickel(II) complex and the disulfidoplatinum(II) complex **4**. Compound **4** can be reconverted into **2** by reduction with the corresponding (nacnac)-nickel(I) precursor, $[\{\text{Ni}(\text{nacnac})\}_2]\cdot\text{toluene}$.

Complex **2** is sensitive toward air and moisture. It reacts readily with dry dioxygen to give the corresponding superoxo(nacnac)nickel(II)^[2c] and disulfidobis(triphenylphosphine)platinum(II) (**4**) complexes as sole products (Scheme 3). Thus complex **4** can be readily prepared from **2** in 77% yield and has been structurally characterized (Figure 6). Remarkably, such disulfide-platinum(II) complexes are rare. The latter species has only previously been detected and spectroscopically characterized by Ishii and co-workers.^[13] Remarkably, compound **4** can be reconverted

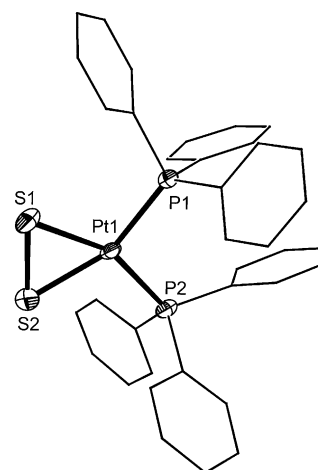


Figure 6. Molecular structure of compound **4**. Thermal ellipsoids are drawn at 50% probability level. Hydrogen atoms are omitted. Selected distances [Å] and angles [°]: Pt1–P1 2.255(2), Pt1–P2 2.284(2), Pt1–S1 2.324(2), Pt1–S2 2.339(2), S1–S2 2.092(3), P1–Pt1–P2 100.34(8), P1–Pt1–S1 103.06(8), P2–Pt1–S1 156.60(9), P1–Pt1–S2 156.34(8), P2–Pt1–S2 103.30(8), S1–Pt1–S2 53.32(9), S2–S1–Pt1 63.72(9).

into complex **2** by treatment of **4** with the nickel(I) precursor $[\{\text{Ni}(\text{nacnac})\}_2]\cdot\text{toluene}^{[7]}$ (see Scheme 3).

Conclusion

The two-electron reduction of the dimeric supersulfido-(nacnac)nickel(II) complex **1** with bis(triphenylphosphine)-ethyleneplatinum(0) furnishes the unique Ni,Pt-subdisulfido complex **2**, which undergoes reversible one-electron oxidation to form the corresponding diamagnetic Ni,Pt-disulfido cation in compound **3** with a S–S single bond. DFT calculations in accordance with spectroscopic (EPR, paramagnetic NMR) and structural features of complex **2** revealed a weak attractive S...S interaction in the S₂ bridge, highlighting significant S₂³⁻ radical character (ca. 41%), very similar to the $\{\text{Cu}_3\text{S}_2\}^{3+}$ system but with strongly unsymmetrical sulfur spin densities owing to a twisted coordination of the S₂ ligand to the Ni center. In fact, this asymmetry is related to the partial reduction of the disulfur ligand beyond the S₂³⁻ state, and thus partial oxidation of nickel beyond Ni^{II}. Furthermore, our computational results predict that the replacement of the redox non-innocent Ni^{II} center in **2** by Zn^{II} generates a heterobimetallic subdisulfido radical complex with “pure” S₂³⁻ character.

Experimental Section

General considerations: All experiments and manipulations were carried out under dry oxygen-free nitrogen by using standard Schlenk techniques or in an MBraun inert atmosphere glovebox containing an atmosphere of purified nitrogen. Solvents were dried by standard methods and freshly distilled prior to use. The starting materials **1**,^[3c] $[(\text{NiL})_2]\cdot\text{toluene}^{[7]}$ (L = CH₃(CMe)(2,6-*i*-Pr₂C₆H₃N))₂, $[\text{Fe}(\text{C}_3\text{H}_5)_2][\text{B}(\text{C}_6\text{F}_5)_4]$,^[14] and $[\text{Pt}(\text{Ph}_3\text{P})_2(\eta^2\text{-C}_2\text{H}_4)]$ ^[15] were prepared according to literature procedures. High-resolution ESI-MS were measured on a Thermo Scientific LTQ orbitrap XL. ¹H and ³¹P NMR spectra were recorded on Bruker spectrometer APX 200 and AV 400, and the corresponding chemical shifts are referenced to the ¹H NMR signal of tetramethylsilane and the ³¹P NMR signal of 85% H₃PO₄.

Single-crystal X-ray structure determinations: Crystals were each mounted on a glass capillary in perfluorinated oil and measured in a cold N₂ flow. The data of compounds **2–4** were collected on an Oxford Diffraction Xcalibur S Sapphire at 150 K (MoK_α radiation, λ = 0.71073 Å). The structures were solved by direct methods and refined on F² with the SHELX-97 software package.^[16] The positions of the hydrogen atoms were calculated and considered isotropically according to a riding model. CCDC-896855 (**2**), 896856 (**3**), and 896857 (**4**) contain the supplementary crystallographic data for this paper. These data can be obtained free of charge from The Cambridge Crystallographic Data Centre via www.ccdc.cam.ac.uk/data_request/cif.

Complex 2: Triclinic, space group *P* $\bar{1}$, *a* = 12.8699(3), *b* = 18.2620(4), *c* = 28.7662(6) Å, α = 80.245(2), β = 79.438(2), γ = 72.610(2)°, *V* = 6295.0(2) Å³, *Z* = 4, ρ_{calcd} = 1.330 Mg m⁻³, μ(MoK_α) = 2.674 mm⁻¹, 45 219 collected reflections, 22 134 crystallographically independent reflections [*R*_{int} = 0.0532], 16 179 reflections with *I* > 2σ(*I*), θ_{max} = 25.00°, *R*(*F*_o) = 0.0562 (*I* > 2σ(*I*)), w*R*(*F*_o²) = 0.1257 (all data), 1335 refined parameters.

Complex 3: Orthorhombic, space group *Pbcn*, *a* = 17.105(1), *b* = 29.104(1), *c* = 39.338(2) Å, α = 90, β = 90, γ = 90°, *V* = 19 608(2) Å³, *Z* = 8, ρ_{calcd} = 1.495 Mg m⁻³, μ(MoK_α) = 1.781 mm⁻¹, 76 731 collected reflections, 17 212 crystallographically independent reflections [*R*_{int} = 0.0981], 10 891

reflections with *I* > 2σ(*I*), θ_{max} = 25°, *R*(*F*_o) = 0.0882 (*I* > 2σ(*I*)), w*R*(*F*_o²) = 0.1570 (all data), 1388 refined parameters.

Complex 4: Triclinic, space group *P* $\bar{1}$, *a* = 11.1674(7), *b* = 12.4848(8), *c* = 16.558(1) Å, α = 92.875(5), β = 109.131(6), γ = 110.834(6)°, *V* = 2001.8(2) Å³, *Z* = 2, ρ_{calcd} = 1.300 Mg m⁻³, μ(MoK_α) = 3.708 mm⁻¹, 14 782 collected reflections, 7017 crystallographically independent reflections [*R*_{int} = 0.0538], 5611 reflections with *I* > 2σ(*I*), θ_{max} = 25°, *R*(*F*_o) = 0.0536 (*I* > 2σ(*I*)), w*R*(*F*_o²) = 0.1369 (all data), 370 refined parameters.

EPR measurements: X-band EPR derivative spectra were recorded on a Bruker ELEXSYS E500 spectrometer equipped with the Bruker standard cavity (ER4102ST) and a helium flow cryostat (Oxford Instruments ESR 910). Microwave frequencies were calibrated with a Hewlett-Packard frequency counter (HP5352B), and the field control was calibrated with a Bruker NMR field probe (ER035M). The spectra were simulated with the program GFIT (by E.B.) for the calculation of the powder spectra with effective *g* values and anisotropic line widths (mixed Lorentzian and Gaussian line shapes were used).

Synthesis of 2

Method A: A solution of $[\text{Pt}(\text{Ph}_3\text{P})_2(\eta^2\text{-C}_2\text{H}_4)]$ (0.83 g, 1.11 mmol) in toluene (15 mL) was added to a cooled (−20°C) solution of **1** (0.60 g, 1.11 mmol) in toluene (15 mL). After stirring for 10 min, the reaction mixture was allowed to warm to room temperature and stirred further for 2 h. In the course of stirring, the color of the solution changed from brown to green. Volatiles were removed in vacuum and the residue was extracted with diethyl ether (5 × 30 mL). After concentration and cooling to −20°C for 24 h, compound **2** crystallized from the solution as dark green crystals (1.15 g, 0.91 mmol, 82%).

Method B: $[\text{Pt}(\text{Ph}_3\text{P})_2\text{S}_2]$ (0.31 g, 0.40 mmol) was added to a cooled (−20°C) solution of $[(\text{NiL})_2]\cdot\text{toluene}$ (0.21 g, 0.20 mmol) in toluene (15 mL). After stirring for 30 min, the reaction mixture was allowed to warm to room temperature and stirred further for 2 h. In the course of stirring the color of the solution changed from red-brown to green. Volatiles were removed in vacuum and the residue was extracted with diethyl ether (3 × 30 mL). After concentration and cooling to −20°C for 24 h, compound **2** crystallized from the solution as dark green crystals (0.45 g, 0.36 mmol, 89%).

Method C: A solution of $[\text{Co}(\text{C}_5\text{Me}_5)_2]$ (0.034 g, 0.10 mmol) in THF (5 mL) was added to a cooled (−70°C) solution of compound **3** (0.20 g, 0.10 mmol) in THF (15 mL). After stirring for 10 min, the reaction mixture was allowed to warm to room temperature and stirred further for 2 h. Volatiles were removed in vacuum and the residue was extracted with diethyl ether (3 × 20 mL). Cooling the concentrated solution to −20°C for 24 h afforded compound **2** as dark green crystals (0.095 g, 0.076 mmol, 73%). M.p. 222°C (decomp.); IR (KBr): $\tilde{\nu}$ = 423 (w), 456 (w), 465 (w), 494 (m), 513 (m), 522 (s), 539 (m), 694 (s), 730 (m), 742 (m), 792 (w), 850 (w), 935 (w), 999 (w), 1028 (w), 1057 (w), 1059 (m), 1159 (w), 1179 (w), 1252 (w), 1317 (m), 1383 (m), 1436 (s), 1461 (w), 1479 (w), 1495 (w), 1525 (w), 1544 (w), 2863 (w), 2923 (m), 2958 (s), 3051 cm⁻¹ (w); HR ESI-MS (ion spray voltage 5 kV, flow rate 5 μL min⁻¹, in THF): *m/z* calcd for C₆₅H₇₂N₂NiS₂P₂Pt [*M*+H]⁺: 1259.36079; found: 1259.35039; elemental analysis calcd (%) for C₆₅H₇₁N₂NiS₂P₂Pt: C 61.95, H 5.68, N 2.22; found: C 61.70, H 5.75, N 2.15. See Figure S1 and S2 as well as Tables S8 and S9 in the Supporting Information for ¹H and ³¹P NMR data and signal assignment.

Synthesis of 3: A solution of $[\text{Fe}(\text{C}_3\text{H}_5)_2][\text{B}(\text{C}_6\text{F}_5)_4]$ (0.34 g, 0.40 mmol) in THF (10 mL) was added to a cooled (−30°C) solution of **2** (0.50 g, 0.40 mmol) in THF (10 mL) with stirring. After addition the reaction mixture was allowed to warm to room temperature and stirred further for 2 h. Volatiles were removed in vacuum and the dark brown residue was washed with *n*-hexane (25 mL) and extracted with benzene (20 mL). After concentration and cooling to 6°C for 48 h, compound **3** crystallized as black crystals (0.69 g, 0.36 mmol, 89%). M.p. 231°C (decomp); ¹H NMR (400.13 MHz, [D₈]THF, 25°C): δ = 1.07 (d, ³*J* (H,H) = 7 Hz, 12H; CHMe₂), 1.18 (d, ³*J* (H,H) = 7 Hz, 12H; CHMe₂), 1.45 (s, 6H; NCMe), 3.73–4.00 (m, 4H; CHMe₂), 5.09 (s, 1H; γ-CH), 6.81–7.43 ppm (m, 36H, Ar-H); ¹³C{¹H} NMR (100.61 MHz, [D₈]THF, 25°C): δ = 21.9, 24.0, 26.4, 29.4 (NCMe, CHMe₂), 101.5 (γ-C), 124.7, 127.7, 141.5, 154.1, 161.5 (NCMe, 2,6-*i*-Pr₂C₆H₃), 129.6, 129.7, 129.8, 132.9, 134.9, 135.0,

135.1 ppm ($P(C_6H_5)_3$): $^{31}P\{^1H\}$ NMR (161.97 MHz, $[D_8]THF$, 25°C): δ 11.6 ppm (^{195}Pt satellites, $^1J(P,Pt) = 3963$ Hz); $^{19}F\{^1H\}$ NMR (188.31 MHz, $[D_8]THF$, 25°C): $\delta = -134.4$ (brs, *o*-F), -166.8 (t, $J(F,F) = 20.2$ Hz, *p*-F), -170.2 (brt, $J(F,F) = 17.6$ Hz, *m*-F); IR (KBr): $\tilde{\nu} = 457$ (w), 499 (w), 510 (m), 522 (m), 544 (m), 573 (w), 602 (w), 610 (w), 661 (w), 683 (m), 692 (m), 707 (w), 744 (w), 756 (w), 768 (w), 775 (w), 799 (w), 981 (s), 1028 (w), 1057 (w), 1093 (s), 1059 (m), 1163 (w), 1180 (w), 1254 (w), 1275 (m), 1316 (m), 1392 (m), 1436 (m), 1464 (s), 1514 (m), 1532 (w), 1588 (w), 1643 (w), 2869 (w), 2927 (w), 2963 (m), 3059 cm^{-1} (w); elemental analysis calcd (%) for $C_{107}H_{89}N_2NiS_2Pt [M+3C_6H_6]^+$: C 59.13, H 4.13, N 1.29; found: C 59.34, H 4.34, N 1.57.

Reaction of 2 with dioxygen and the formation of 4: A solution of **2** (0.54 g, 0.43 mmol) in toluene (20 mL) was cooled to 0°C. The N_2 atmosphere in the flask was exchanged with dried oxygen. After stirring for 10 min, the reaction mixture was allowed to warm to room temperature and stirred further for 1 h under the oxygen atmosphere. In the course of stirring a pink precipitate of compound **4** was formed. After filtration, the filtrate was concentrated and cooled to $-20^\circ C$ to afford $[LNiO_2]^{2+}$ as green crystals (0.15 g, 0.29 mmol, 67%). The pink precipitate of **4** was collected and dried in vacuum (0.26 g, 0.33 mmol, 77%). Single crystals of **4** were obtained from a toluene solution at 4°C. Analytical data for compound **4**: M.p. 202°C (decomp.); 1H NMR (200.13 MHz, $CDCl_3$, 25°C): $\delta = 7.13$ – 7.41 ppm (m, Ar-H); $^{13}C\{^1H\}$ NMR (100.61 MHz, $CDCl_3$, 25°C): $\delta = 127.9$, 128.0, 128.1, 130.4, 133.9, 134.0, 134.2 ppm (Ar-C); $^{31}P\{^1H\}$ NMR (161.97 MHz, $CDCl_3$, 25°C): $\delta = 22.5$ ppm (^{195}Pt satellites, $^1J(P,Pt) = 3943$ Hz); HR ESI-MS (ion spray voltage 5 kV, flow rate 5 $\mu L \cdot min^{-1}$, in THF): m/z calcd for $C_{36}H_{30}S_2Pt [M]^+$: 783.09064; found: 783.09346.

Computational methods: All structures were optimized at the RI-BP86/def2-TZVP level of theory by using the TURBOMOLE program package.^[17] That is, the generalized gradient approximation (GGA) of the Becke exchange functional^[18] and the Perdew correlation functional^[19] (BP86), in conjunction with standard TURBOMOLE all-electron def2-TZVP basis sets^[20] for atoms with $Z < 36$ were used, together with an approximation of the Coulomb term by density fitting^[21] with a def2-TZVP auxiliary basis set. For the Pt atom a quasirelativistic small-core pseudopotential^[22] (ECP) with the corresponding valence basis set^[20] of the quality (8s7p6d1f)/[6s4p3d1f] was employed. The unrestricted Kohn–Sham formalism was used for all open-shell species. The crystal structures of complex **2** and the $[(tmeda)_3Cu_3S_3]^{3+}$ complex were used as initial structures for full optimization. For comparison, partial optimization of only the hydrogen-atom positions for the X-ray-based structure of **2** was also done at the RI-BP86/def2-TZVP level (denoted as “crystal/opt-H” in the Supporting Information).

g-Tensor calculations were performed in the MAG-ReSpect program^[23] at one-component second-order perturbation level^[24] by using a common gauge origin (see Tables S5 and S6 in the Supporting Information) and a coupled-perturbed Kohn–Sham (CPKS) treatment for hybrid functionals,^[25] together with a small-core scalar relativistic pseudopotential (ECP) for the Pt atom in the SCF step and a corresponding spin-orbit (SO) ECP in the calculation of the SO matrix elements (related to Pt SO coupling). For Ni and Zn we employed modified TZVP all-electron basis sets of the (15s11p6d)/[9s7p4d] quality,^[26] whereas ligand atoms were treated by Huzinaga–Kutzelnigg-type IGLO-II basis sets.^[27] To assess the effect of exact Hartree–Fock (HF) exchange admixture, several exchange-correlation functionals have been tested: BP86 with 0%, the B3LYP** global hybrid with 10%, and B3LYP with 20% exact-exchange admixture.^[28] All SO matrix elements (except for the SO ECP on Pt) have been obtained within the accurate and efficient atomic mean-field approximation (AMFI)^[29,30] to the full many-electron Breit–Pauli SO operator.

The NMR shielding tensor calculations for paramagnetic systems were carried out with an in-house PNMR program,^[31] based on our recent approach, which also includes all relevant terms, going beyond the dominant contact shifts.^[10] For this purpose, the orbital term σ_{orb} and EPR hyperfine coupling tensors were computed in the Gaussian 09 program package,^[32] the former by an open-shell generalization of the usual CPKS procedures for the diamagnetic case, by using gauge-including atomic or-

bitals (GIAO).^[33] These calculations have been done with the same exchange-correlation functionals and basis sets as the *g*-tensor calculations (see above). All temperature-dependent terms were computed at 298 K. The calculated 1H and ^{31}P NMR shieldings were converted to chemical shifts (δ in [ppm]) relative to the shieldings of tetramethylsilane (TMS) and PH_3 as a secondary standard ($\delta(^{31}PH_3) = -266.1$ ppm),^[34] respectively, obtained at the same computational level. The calculated NMR shifts were averaged over magnetically equivalent nuclei.

Atomic charges and spin densities were evaluated at the B3LYP**/TZVP level of theory by means of natural population analyses (NPA), by using the built-in NBO subroutines of the Gaussian 09 program.^[35] Spin densities are provided either as isosurface plots or as NPA atomic values. Mayer bond orders^[36] were evaluated by using the program BORDER.^[37] The wave functions were also analyzed in the DGrid program^[38] by means of the electron localization function (ELF),^[39] the electron localizability indicator based on the parallel-spin electron pair density (ELI-D),^[40] and the quantum theory of atoms in molecules (QTAIM).^[41] For this purpose, the Kohn–Sham orbitals of the single-point calculations were transferred to the DGrid and the examined property was calculated on a grid with ten points per Bohr. The results of ELF, ELI-D, and QTAIM analyses were visualized by using the ParaView program.^[42] The visualization of molecules, spin density distributions, and orbitals was done with Molekel^[43] and gOpenMol.^[44]

Acknowledgements

The authors acknowledge support from the Cluster of Excellence “Unifying Concepts in Catalysis” (<http://www.unicat.tu-berlin.de>) funded by the German Research Foundation—Deutsche Forschungsgemeinschaft (DFG) and the Senate of Science and Education of the State of Berlin (Program “Nachhaltige Chemie”). P.H. also thanks the Alexander von Humboldt Foundation and the Slovak grant agency VEGA (project No. 2/0079/09) for financial support.

- 1) a) S. Ferguson-Miller, G. T. Babcock, *Chem. Rev.* **1996**, *96*, 2889; b) E. Kim, M. E. Helton, I. M. Wasser, K. D. Karlin, S. Lu, H.-W. Huang, P. Moenne-Loccoz, C. D. Incarvito, A. L. Rheingold, M. Honecker, S. Kaderli, A. D. Zuberbühler, *Proc. Natl. Acad. Sci. USA* **2003**, *100*, 3623; c) A. Decker, E. I. Solomon, *Curr. Opin. Chem. Biol.* **2005**, *9*, 152; d) A. Müller, W. Jaegermann, J. H. Enemark, *Coord. Chem. Rev.* **1982**, *46*, 245; e) T. Punniyamurthy, S. Velusamy, J. Iqbal, *Chem. Rev.* **2005**, *105*, 2329; f) B. Meunier, *Biomimetic Oxidations Catalyzed by Transition Metals*, Imperial College Press, London **2000**; g) M. R. Dubois, *Chem. Rev.* **1989**, *89*, 1; h) I. Bar-Nahum, J. T. York, V. G. Young Jr., W. B. Tolman, *Angew. Chem.* **2008**, *120*, 543; *Angew. Chem. Int. Ed.* **2008**, *47*, 533; i) S. Yao, M. Driess, *Acc. Chem. Res.* **2012**, *45*, 276.
- 2) Selected superoxo complexes: a) C. J. Cramer, W. B. Tolman, K. H. Theopold, A. L. Rheingold, *Proc. Natl. Acad. Sci. USA* **2003**, *100*, 3635, and cited references therein; b) M. T. Kieber-Emmons, C. G. Riordan, *Acc. Chem. Res.* **2007**, *40*, 618; c) S. Yao, E. Bill, C. Milsman, K. Wieghardt, M. Driess, *Angew. Chem.* **2008**, *120*, 7218; *Angew. Chem. Int. Ed.* **2008**, *47*, 7110; d) J. Shearer, N. Zhao, *Inorg. Chem.* **2006**, *45*, 9637; e) R. Huacuja, D. J. Graham, C. M. Fafard, C.-H. Chen, B. M. Foxman, D. E. Herbert, G. Alliger, C. M. Thomas, O. V. Ozerov, *J. Am. Chem. Soc.* **2011**, *133*, 3820.
- 3) Selected supersulfido complexes: a) R. C. Elder, M. Trkula, *Inorg. Chem.* **1977**, *16*, 1048; b) M. M. Taqui Khan, M. R. H. Siddiqui, *Inorg. Chem.* **1991**, *30*, 1157; c) S. Yao, C. Milsman, E. Bill, K. Wieghardt, M. Driess, *J. Am. Chem. Soc.* **2008**, *130*, 13536; superselenido complex: d) S. L. Yao, Y. Xiong, X. H. Zhang, M. Schlangen, H. Schwarz, C. Milsman, M. Driess, *Angew. Chem.* **2009**, *121*, 4621; *Angew. Chem. Int. Ed.* **2009**, *48*, 4551.
- 4) a) E. C. Brown, J. T. York, W. E. Antholine, E. Ruiz, S. Alvarez, W. B. Tolman, *J. Am. Chem. Soc.* **2005**, *127*, 13752; b) C. Mealli, A.

- Ienco, A. Poduska, R. Hoffmann, *Angew. Chem.* **2008**, *120*, 2906; *Angew. Chem. Int. Ed.* **2008**, *47*, 2864; c) S. Alvarez, R. Hoffmann, C. Mealli, *Chem. Eur. J.* **2009**, *15*, 8358; d) J. F. Berry, *Chem. Eur. J.* **2010**, *16*, 2719; e) R. Sarangi, L. Yang, S. G. Winikoff, L. Gagliardi, C. J. Cramer, W. B. Tolman, E. I. Solomon, *J. Am. Chem. Soc.* **2011**, *133*, 17180; f) S. Alvarez, E. Ruiz, *Chem. Eur. J.* **2010**, *16*, 2726.
- [5] A. P. Cole, D. E. Root, P. Mukherjee, E. I. Solomon, T. D. P. Stack, *Science* **1996**, *273*, 1848.
- [6] a) H. Sitzmann, D. Saurenz, G. Wolmershauser, A. Klein, R. Boese, *Organometallics* **2001**, *20*, 700; b) S. A. Yao, K. M. Lancaster, A. W. Götz, S. DeBeer, J. F. Berry, *Chem. Eur. J.* **2012**, *18*, 9179.
- [7] G. Bai, P. Wei, D. W. Stephan, *Organometallics* **2005**, *24*, 5901.
- [8] a) J. Chatt, D. M. P. Mingos, *J. Chem. Soc. A* **1970**, 1243; b) V. W.-W. Yam, P. K.-Y. Yeung, K.-K. Cheung, *J. Chem. Soc. Chem. Commun.* **1995**, 267; c) M. Capdevila, Y. Carrasco, W. Clegg, R. A. Coxall, P. González-Duarte, A. Lledós, J. Sola, G. Ujaque, *Chem. Commun.* **1998**, 597; d) A. Ienco, M. Caporali, F. Zanobini, C. Mealli, *Inorg. Chem.* **2009**, *48*, 3840; e) V. M. Iluc, C. A. Laskowski, C. K. Brozek, N. D. Harrold, G. L. Hillhouse, *Inorg. Chem.* **2010**, *49*, 6817.
- [9] a) D. F. Evans, *J. Chem. Soc.* **1959**, 2003; b) T. Ayers, R. Turk, C. Lane, J. Goins, D. Jameson, S. J. Slattery, *Inorg. Chim. Acta* **2004**, *357*, 202.
- [10] P. Hrobárik, R. Reviakine, A. V. Arbuznikov, O. L. Malkina, V. G. Malkin, F. H. Köhler, M. Kaupp, *J. Chem. Phys.* **2007**, *126*, 024107.
- [11] M. Reiher, O. Salomon, B. A. Hess, *Theor. Chem. Acc.* **2001**, *107*, 48.
- [12] A. Poduska, R. Hoffmann, A. Ienco, C. Mealli, *Chem. Asian J.* **2009**, *4*, 302.
- [13] A. Ishii, M. Murata, H. Oshida, K. Matsumoto, J. Nakayama, *Eur. J. Inorg. Chem.* **2003**, 3716.
- [14] a) A. Nafady, T. T. Chin, W. E. Geiger, *Organometallics* **2006**, *25*, 1654; b) N. G. Connelly, W. E. Geiger, *Chem. Rev.* **1996**, *96*, 877.
- [15] R. A. Head, *Inorg. Synth.* **1990**, *28*, 132.
- [16] SHELX-97, Program for Crystal Structure Determination, G. M. Sheldrick, Universität Göttingen (Germany), **1997**.
- [17] TURBOMOLE, version 6.3.1, a Development of University of Karlsruhe and Forschungszentrum Karlsruhe GmbH, **1989–2007**, TURBOMOLE GmbH since **2007**; available from <http://www.turbomole.com>.
- [18] A. D. Becke, *Phys. Rev. A* **1988**, *38*, 3098.
- [19] a) J. P. Perdew, Y. Wang, *Phys. Rev. B* **1986**, *33*, 8822; b) J. P. Perdew, Y. Wang, *Phys. Rev. B* **1986**, *34*, 7406.
- [20] F. Weigend, R. Ahlrichs, *Phys. Chem. Chem. Phys.* **2005**, *7*, 3297.
- [21] F. Weigend, *Phys. Chem. Chem. Phys.* **2006**, *8*, 1057.
- [22] D. Andrae, U. Haussermann, M. Dolg, H. Stoll, H. Preuss, *Theor. Chim. Acta* **1990**, *77*, 123.
- [23] MAG-ReSpect, version 2.1, V. G. Malkin, O. L. Malkina, R. Reviakine, A. V. Arbuznikov, M. Kaupp, B. Schimmelpfennig, I. Malkin, M. Repisky, S. Komorovsky, P. Hrobárik, E. Malkin, T. Helgaker, K. Ruud, **2005**.
- [24] O. L. Malkina, J. Vaara, B. Schimmelpfennig, M. Munzarova, V. G. Malkin, M. Kaupp, *J. Am. Chem. Soc.* **2000**, *122*, 9206.
- [25] M. Kaupp, R. Reviakine, O. L. Malkina, A. Arbuznikov, B. Schimmelpfennig, V. G. Malkin, *J. Comput. Chem.* **2002**, *23*, 794.
- [26] M. Munzarová, M. Kaupp, *J. Phys. Chem. A* **1999**, *103*, 9966.
- [27] W. Kutzelnigg, U. Fleischer, M. Schindler, *The IGLO-Method: Ab Initio Calculation and Interpretation of NMR Chemical Shifts and Magnetic Susceptibilities in NMR Basic Principles and Progress*, Vol. 23 (Eds.: P. Diehl, E. Fluck, H. Günther, R. Kosfeld, J. Seelig), Springer, Berlin/Heidelberg, **1991**, pp. 165–262.
- [28] a) A. D. Becke, *J. Chem. Phys.* **1993**, *98*, 5648; b) C. T. Lee, W. T. Yang, R. G. Parr, *Phys. Rev. B* **1988**, *37*, 785; c) P. J. Stephens, F. J. Devlin, C. F. Chabalowski, M. J. Frisch, *J. Phys. Chem.* **1994**, *98*, 11623.
- [29] B. A. Hess, C. M. Marian, U. Wahlgren, O. Gropen, *Chem. Phys. Lett.* **1996**, *251*, 365.
- [30] AMFI, Atomic Spin-Orbit Mean-Field Integral Program, B. Schimmelpfennig, Stockholms Universitet, Stockholm (Sweden), **1996**.
- [31] PNMNR, a computer program for the calculation of paramagnetic NMR shielding tensors, version 1.0, P. Hrobárik, Technical University of Berlin (Germany), **2011**.
- [32] Gaussian 09, Revision A.02, M. J. Frisch, G. W. Trucks, H. B. Schlegel, G. E. Scuseria, M. A. Robb, J. R. Cheeseman, G. Scalmani, V. Barone, B. Mennucci, G. A. Petersson, H. Nakatsuji, M. Caricato, X. Li, H. P. Hratchian, A. F. Izmaylov, J. Bloino, G. Zheng, J. L. Sonnenberg, M. Hada, M. Ehara, K. Toyota, R. Fukuda, S. Hasegawa, M. Ishida, T. Nakajima, Y. Honda, O. Kitao, H. Nakai, T. Vreven, J. A. Montgomery, Jr., J. E. Peralta, F. Ogliaro, M. Bearpark, J. J. Heyd, E. Brothers, K. N. Kudin, V. N. Staroverov, R. Kobayashi, J. Normand, K. Raghavachari, A. Rendell, J. C. Burant, S. S. Iyengar, J. Tomasi, M. Cossi, N. Rega, J. M. Millam, M. Klene, J. E. Knox, J. B. Cross, V. Bakken, C. Adamo, J. Jaramillo, R. Gomperts, R. E. Stratmann, O. Yazyev, A. J. Austin, R. Cammi, C. Pomelli, J. W. Ochterski, R. L. Martin, K. Morokuma, V. G. Zakrzewski, G. A. Voth, P. Salvador, J. J. Dannenberg, S. Dapprich, A. D. Daniels, Ö. Farkas, J. B. Foresman, J. V. Ortiz, J. Cioslowski, D. J. Fox, Gaussian, Inc., Wallingford CT, **2009**.
- [33] K. Wolinski, J. F. Hinton, P. Pulay, *J. Am. Chem. Soc.* **1990**, *112*, 8251.
- [34] C. J. Jameson, A. Dedios, A. K. Jameson, *Chem. Phys. Lett.* **1990**, *167*, 575.
- [35] A. E. Reed, L. A. Curtiss, F. Weinhold, *Chem. Rev.* **1988**, *88*, 899.
- [36] a) I. Mayer, *Chem. Phys. Lett.* **1983**, *97*, 270; b) I. Mayer, *Chem. Phys. Lett.* **1985**, *117*, 396.
- [37] BORDER, version 1.0, I. Mayer, Chemical Research Center, Hungarian Academy of Sciences, Budapest, **2005**; available from <http://occam.chemres.hu/programs>.
- [38] DGrid, version 4.6, M. Kohout, Radebeul, **2011**.
- [39] a) A. D. Becke, K. E. Edgecombe, *J. Chem. Phys.* **1990**, *92*, 5397; b) A. Savin, O. Jepsen, J. Flad, O. K. Andersen, H. Preuss, H. G. von Schnering, *Angew. Chem.* **1992**, *104*, 186; *Angew. Chem. Int. Ed. Engl.* **1992**, *31*, 187; c) M. Kohout, A. Savin, *Int. J. Quantum Chem.* **1996**, *60*, 875.
- [40] a) M. Kohout, *Int. J. Quantum Chem.* **2004**, *97*, 651; b) M. Kohout, K. Pernal, F. R. Wagner, Y. Grin, *Theor. Chem. Acc.* **2004**, *112*, 453.
- [41] R. F. W. Bader, *Atoms in Molecules: A Quantum Theory*, Oxford University Press, Oxford, **1990**.
- [42] ParaView, version 3.8, Kitware Inc., Clifton Park, New York (USA), **2010**; available from <http://www.paraview.org>.
- [43] Molekel, version 5.4, U. Varetto, Swiss National Supercomputing Centre, Manno (Switzerland), **2009**; available from: <http://molekel.cscs.ch>.
- [44] gOpenMol, version 3.0, L. Laaksonen, CSC, Espoo (Finland), **2005**; available from <http://www.csc.fi/english/pages/gOpenMol>.

Received: October 11, 2012
Published online: December 18, 2012